Available online at www.sciencedirect.com
SCIENCE DIRECT®
International Journal of Heat and Mass Transfer 47 (2004) 4745–4759
International Journal of HEAT and MASS TRANSFER
www.elsevier.com/locate/ijhmt

Interacting effects of uniform flow, plane shear, and near-wall proximity on the heat and mass transfer of respiratory aerosols

P. Worth Longest [a,*], Clement Kleinstreuer [b]

[a] Department of Mechanical Engineering, Virginia Commonwealth University, 601 West Main Street, P.O. Box 843015, Richmond, VA 23284-3015, USA
[b] Department of Mechanical and Aerospace Engineering, North Carolina State University, Box 7910, Raleigh, NC 27695, USA

Received 7 April 2004; received in revised form 20 May 2004

Abstract

Individual and interacting effects of uniform flow, plane shear, and near-wall proximity on spherical droplet heat and mass transfer have been assessed for low Reynolds number conditions beyond the creeping flow regime. Validated resolved volume simulations were used to compute heat and mass transfer surface gradients of two-dimensional axisymmetric droplets and three-dimensional spherical droplets near planar wall boundaries for conditions consistent with inhalable aerosols ($5 \leqslant d \leqslant 300$ μm) in the upper respiratory tract. Results indicate that planar shear significantly impacts droplet heat and mass transfer for shear-based Reynolds numbers greater than 1, which occur for near-wall respiratory aerosols with diameters in excess of 50 μm. Wall proximity is shown to significantly enhance heat and mass transfer due to conduction and diffusion at separation distances less than five particle diameters and for small Reynolds numbers. For the Reynolds number conditions of interest, significant non-linear effects arise due to the concurrent interaction of uniform flow and shear such that linear superposition of Sherwood or Nusselt number terms is not allowable. Based on the validated numeric simulations, multivariable Sherwood and Nusselt number correlations are provided to account for individual flow characteristics and concurrent non-linear interactions of uniform flow, planar shear, and near-wall proximity. These heat and mass transfer correlations can be applied to effectively compute condensation and evaporation rates of potentially toxic or therapeutic aerosols in the upper respiratory tract, where non-uniform flow and wall proximity are expected to significantly affect droplet transport, deposition, and vapor formation.

Keywords: Droplet heat and mass transfer; Respiratory aerosols; Near-wall droplet evaporation; Droplet Nusselt and Sherwood number correlations

1. Introduction

Individual and concurrent interaction effects from uniform flow, plane shear, and near-wall proximity may significantly influence particle or droplet heat and mass transfer characteristics in a number of

* Corresponding author. Tel.: +1 804 827 7023; fax: +1 804 827 7030.
E-mail address: pwlongest@vcu.edu (P.W. Longest).

0017-9310/$ - see front matter © 2004 Elsevier Ltd. All rights reserved.
doi:10.1016/j.ijheatmasstransfer.2004.05.029

Nomenclature

A	surface area
C_p	specific heat at constant pressure
d	droplet diameter
D_s	binary diffusion coefficient in air
$\sqrt{g}$	metric tensor determinate
h	convective heat transfer coefficient
h_m	convective mass transfer coefficient
h/d	non-dimensional wall distance
k_g	thermal conductivity of gas
L_s	latent heat of vaporization of species
m_d	droplet mass
n	outward normal direction
n_s	mass flux of species s
Nu	Nusselt number
p	pressure
Pr	Prandtl number
P_{sat}	saturation pressure
q_{conv}	convective heat flux
r	droplet radius
R_s	gas constant
Re_p	uniform flow Reynolds number
Re_g	shear-based Reynolds number
Sc	Schmidt number
Sh	Sherwood number
t	time
T	temperature
u_∞	uniform upstream velocity
u_i	local velocity component
x_i	spatial coordinate
$\tilde{x}_i$	moving mesh location
x_s	mole fraction of component s

Greek symbols

$\dot{\gamma}$	shear rate
μ	absolute viscosity
ρ	density
ω_s	mass fraction of species s

Subscripts

d	droplet or liquid
g	gas
i, j, k	index notation
s	droplet component or species
surf	droplet surface
∞	upstream conditions

applications. In particular, volatile droplet evaporation and hygroscopicity, or water condensation, influence the transport and deposition of respiratory aerosols [1–3] including potentially toxic pollutants [4,5], as well as the generation and delivery of inhaled therapeutics [6,7]. Efficient models for droplet heat and mass transfer, including respiratory aerosol condensation and evaporation, require predefined Sherwood and Nusselt number correlations to represent the external flow conditions of interest. For a wide range of applications, including combustion, the effects of non-uniform flow and wall proximity on droplet heat and mass transfer have been considered as reviewed by Clift et al. [8], Sadhal et al. [9], and Sirignano [10], among others. These previous studies largely focused on either creeping flow or high Reynolds number conditions. However, Sherwood and Nusselt number correlations are not available for the concurrent interaction of intermediate uniform and plane shear flows in the presence of a conducting or absorbing boundary consistent with depositing aerosols in the respiratory tract.

For wall-bounded shear flows at low and high Reynolds numbers, analytic solutions have been evaluated for particle lift [11–13] as well as heat and mass transfer [14,15]. A majority of studies that addressed the influence of boundaries and shear on heat and mass transfer considered cylindrical walls with diameters on the same order of magnitude as the spherical particle [8]. A notable exception was provided by Frenkel and Acrivos [16], who applied a singular perturbation approach to determine Nusselt number values for a spherical particle in plane shear flow. The resulting correlation predicted a significant effect of plane shear on particle heat and mass transfer for creeping flow conditions. However, the presence of a boundary wall and superimposed uniform velocity were not considered.

Direct numerical simulations have frequently been used to evaluate the heat and mass transfer characteristics of particles and droplets for conditions where analytic solutions are not available. These resolved volume techniques have been used to directly assess the effects of linear droplet arrays [17,18], variable gas-phase properties [19], and three-dimensional droplet arrays [20]. Considering the influence of non-uniform flow, Dandy and Dwyer [21] computed three-dimensional resolved volume simulations to investigate the effects of plane shear on particle drag, lift, and transport characteristics. For the limited range of shear rates considered, Dandy and Dwyer [21] found that heat and mass transfer depended predominately on the uniform flow Reynolds number. In a similar numeric study, Nirschl et al. [22] considered the influence of both plane shear flow and near-wall proximity on particle heat and mass transfer. Significant variations of the Nusselt number were

observed for shear Reynolds numbers greater than 1 and for particles within three diameters of the wall. Furthermore, the results of Nirschl et al. [22] indicated that particle rotation had a negligible effect on heat and mass transfer for shear-based Reynolds numbers less than approximately 30. However, the influence of concurrent uniform flow was not considered, and Nusselt number correlations were not provided.

Studies dealing with respiratory aerosols typically focus on particle diameters less than 10 μm. This is based on the effective filtering mechanism of the lung and supporting evidence that only a small percentage of particles greater than 10 μm reach the alveolar or pulmonary region during moderate breathing conditions [6,23,24]. However, particles on the order of 100–300 μm are frequently inhaled through the mouth and nose, i.e., the inhalation efficiency of 100 μm droplets is approximately 50% [25,26]. Nearly all of the inhaled particles in this size range are deposited in the nasal and oral cavities or the pharynx [23]. Analysis of toxic and therapeutic doses within these extrathoracic regions requires accurate assessments of aerosol transport and deposition, which are largely influenced by evaporation [3] and water condensation [2]. Moreover, larger particles deliver a significantly greater dose of toxic or therapeutic compound. For aerosols within a 100–300 μm size range, uniform flow Reynolds numbers are expected to be on the order of $Re_p \leqslant 8$ for inhalation in the upper respiratory tract from ambient conditions. Maximum shear values in the upper respiratory tract may reach 6000 s^{-1} during moderate to heavy breathing. The resulting maximum shear-based Reynolds number (Re_g) is approximately 32.

To effectively compute the heat and mass transfer characteristics of respiratory aerosols, including evaporation and condensation, Sherwood and Nusselt number correlations for non-uniform and near-wall conditions are necessary. In this study, resolved volume simulations have been employed to investigate the interacting effects of uniform flow, plane shear, and wall proximity on the heat and mass transfer of idealized spherical non-rotating droplets. Conditions of interest include particle diameters $5 \leqslant d \leqslant 300$ μm, uniform flow Reynolds numbers $0 \leqslant Re_p \equiv \rho u_\infty d/\mu \leqslant 8$ and shear-based Reynolds numbers $0 \leqslant Re_g \equiv \rho \dot{\gamma} d^2/\mu \leqslant 32$. Smaller droplet sizes have been neglected in this study due to potential non-continuum effects on heat and mass transfer. It is hypothesized that shear stress will significantly influence the heat and mass transfer of larger droplets, whereas wall proximity will play a predominate role in the transport field surrounding smaller droplets. Moreover, the interaction of uniform and shear flow is expected to be complex due to the violation of creeping flow conditions such that linear superposition of Sherwood and Nusselt number terms is not allowable. Based on validated numerical computations, Sherwood and Nusselt number correlations are provided to account for individual flow field characteristics and concurrent non-linear interactions of uniform flow, plane shear, and near-wall proximity.

2. Methods

2.1. Droplet evaporation and assumptions

The evaporation and condensation of volatile and hygroscopic respiratory aerosols is typically modeled with a semi-empirical approach in which Sherwood and Nusselt number correlations are used to account for gas-phase transport [1–3]. Due to the relatively slow evaporation rates of droplets that are consistent with respiratory aerosols, rapid mixing assumptions are typically implemented for the discrete liquid phase [27,28]. That is, infinite conduction and diffusion are assumed within the droplet such that liquid temperature and concentrations are spatially constant but vary with time [10]. The semi-empirical approach requires solution of a coupled set of ordinary differential equations (ODEs) for heat and mass conservation, which can be numerically computed very efficiently. However, this ODE-based approach may not be valid for conditions that violate the assumptions of the underlying empirical approximations.

To extend the computationally efficient semi-empirical approach to non-uniform flow conditions, resolved volume simulations have been employed to evaluate appropriate Sherwood and Nusselt number values. These computational solutions directly simulate (or fully resolve) the gas-phase field around an evaporating droplet including heat and mass transfer. Comparisons of both resolved volume simulations and semi-empirical solutions to empirical droplet evaporation data indicate that the rapid mixing assumptions may be applied for the respiratory aerosol conditions of interest [27,28]. Furthermore, Longest and Kleinstreuer [28] modeled liquid droplet conduction and showed that accounting for internal temperature gradients had a negligible effect on respiratory aerosol evaporation rates. In contrast, time variations in droplet temperature associated with evaporative cooling were shown to significantly impact droplet evaporation. To accurately compute the droplet wet-bulb temperature, transient resolved volume simulations have been conducted and gas-phase surface transport gradients have been assessed once pseudo-steady-state conditions are reached. This time varying methodology allows for an effective computation of surface blowing velocity effects, which may become important for some of the higher Reynolds numbers considered. Furthermore, the implementation of a transient resolved volume code allows for direct validation of the simulations by comparison with empirical droplet evaporation results.

In addition to the rapid mixing model, a number of other simplifying assumptions can be applied for respiratory aerosol conditions. The relatively small droplet diameters of interest and low to moderate particle Reynolds numbers result in dominate surface tension forces, allowing for the assumption of spherically symmetric droplets [8,9]. Constant surface temperature and concentration values have been assumed based on expected rapid mixing within the droplet [27]. In addition, Niazmond et al. [29] have shown that the thermal Marangoni effect induces significant surface flows, arising from temperature dependent variations in surface tension, that aid in equalizing droplet surface temperatures and concentrations [20]. For the gas-phase, the assumptions of low mass fluxes and dilute chemical species have been made. Reynolds and Mach number conditions as well as moderate temperature variations allow for the assumptions of laminar incompressible flow [30]. Gas-phase properties have been assumed spatially constant and calculated at the film temperature, except for the saturation pressure of the evaporating species, which is evaluated at the current droplet temperature.

2.2. Governing equations and numerical methods

Conservation of energy for an immersed single component droplet, indicated by the subscript d, under rapid mixing model conditions can be expressed as

$$\frac{\mathrm{d}T}{\mathrm{d}t} m_{\mathrm{d}} C_{p\mathrm{d}} = -\int_{\mathrm{surf}} q_{\mathrm{conv}}\,\mathrm{d}A - \int_{\mathrm{surf}} n_{\mathrm{s}} L_{\mathrm{s}}\,\mathrm{d}A \tag{1}$$

In the above equation, m_{d} is the droplet mass, $C_{p\mathrm{d}}$ is the liquid specific heat, q_{conv} is the convective heat flux, n_{s} is the mass flux of the evaporating chemical species at the droplet surface, and L_{s} is the latent heat of vaporization of the liquid component. The integrals are performed over the droplet surface area, A. Conservation of mass for an immersed droplet based on evaporating flux can be expressed as

$$\frac{\mathrm{d}(m_{\mathrm{d}})}{\mathrm{d}t} = -\int_{\mathrm{surf}} n_{\mathrm{s}}\,\mathrm{d}A \tag{2a}$$

Implementing the chain rule, Eq. (2a) is often rewritten in terms of droplet radius [31]

$$\frac{\mathrm{d}r}{\mathrm{d}t} = -\frac{\int_{\mathrm{surf}} n_{\mathrm{s}}\,\mathrm{d}A}{A\rho_{\mathrm{s}}} \tag{2b}$$

with $r(t=0)=R_0$.

For semi-empirical approximations, heat and mass fluxes under uniform flow conditions are often based on the Sherwood number correlation developed by Ranz and Marshall [32] valid for $2 \leqslant Re_{\mathrm{p}} \leqslant 200$

$$Sh = 2.0 + 0.6 Re_{\mathrm{p}}^{1/2} Sc^{1/3} \tag{3a}$$

where the uniform flow Reynolds number is defined as $Re_{\mathrm{p}} = \rho u_{\infty} d/\mu$. Blowing effects are absent in this expression, which is attributed to the fact that the observations by Ranz and Marshall [32] were mostly below 90 °C [33]. At non-zero Reynolds numbers, experimental observations show a strong analogy between heat and mass transfer allowing for a corresponding Nusselt number correlation of

$$Nu = 2.0 + 0.6 Re_{\mathrm{p}}^{1/2} Pr^{1/3} \tag{3b}$$

The analogy between heat and mass transfer expressions is not exact largely due to property variations in the gas-phase associated with moderate to high flux rates [8]. In a more recent analysis, Clift et al. [8] correlated available data for $Re_{\mathrm{p}} < 400$ with the expressions

$$Nu = 1 + (1 + Re_{\mathrm{p}} Pr)^{1/3} \max[1, Re_{\mathrm{p}}^{0.077}] \tag{4a}$$

and

$$Sh = 1 + (1 + Re_{\mathrm{p}} Sc)^{1/3} \max[1, Re_{\mathrm{p}}^{0.077}] \tag{4b}$$

Once Sherwood and Nusselt numbers have been determined, the associated dimensional heat and mass transfer parameters can be computed from

$$h = \frac{Nuk_{\mathrm{g}}}{d} \quad \text{and} \quad h_{\mathrm{m}} = \frac{ShD_{\mathrm{s}}}{d} \tag{5a,b}$$

where k_{g} is the thermal conductivity of the gas and D_{s} is the binary diffusion coefficient of species s with air. For the semi-empirical solution, these transport coefficients are employed to evaluate the mean fluxes at the droplet surface, i.e.,

$$\int_{\mathrm{surf}} q_{\mathrm{conv}}\,\mathrm{d}A = \bar{q}_{\mathrm{conv}} \cdot A = hA(T_{\mathrm{d}} - T_{\infty}) \tag{6}$$

and, accounting for the convective effect of droplet evaporation (blowing velocity)

$$\int_{\mathrm{surf}} n_{\mathrm{s}}\,\mathrm{d}A = \bar{n}_{\mathrm{s}} \cdot A = \rho_{\mathrm{g}} h_{\mathrm{m}} A \frac{\omega_{\mathrm{s,surf}} - \omega_{\mathrm{s},\infty}}{1 - \omega_{\mathrm{s,surf}}} \tag{7a}$$

where ω_{s} is the gas-phase mass fraction of the dilute chemical species and ρ_{g} is the gas mixture density, assumed to be that of air. Surface mass flux is often expressed in the following equivalent form

$$\bar{n}_{\mathrm{s}} = \rho_{\mathrm{g}} h_{\mathrm{m}} \ln\left(\frac{1 - \omega_{\mathrm{s},\infty}}{1 - \omega_{\mathrm{s,surf}}}\right) \tag{7b}$$

which arises from an ambient solution ($Re_{\mathrm{p}} = 0$) of the species conservation equation.

Using the resolved volume approach, heat and mass fluxes at the liquid–gas interface can be directly determined from a numerical solution of the surrounding flow field. The gas-phase conservation equations for laminar incompressible flow on a moving mesh in strong conservation law format can be written [34]:

Conservation of mass

$$\frac{\rho_g}{\sqrt{g}}\frac{\partial}{\partial t}(\sqrt{g}) + \rho_g \frac{\partial}{\partial x_j}\left(u_j - \frac{\partial \tilde{x}_j}{\partial t}\right) = 0 \tag{8a}$$

Conservation of momentum

$$\frac{\rho_g}{\sqrt{g}}\frac{\partial}{\partial t}(\sqrt{g}u_i) + \rho_g \frac{\partial}{\partial x_j}\left[\left(u_j - \frac{\partial \tilde{x}_j}{\partial t}\right)u_i\right] = -\frac{\partial p}{\partial x_i} + \mu\frac{\partial^2 u_i}{\partial x_j^2} \tag{8b}$$

Conservation of energy

$$\frac{\rho_g C_{pg}}{\sqrt{g}}\frac{\partial}{\partial t}(\sqrt{g}T) + C_{pg}\rho_g \frac{\partial}{\partial x_j}\left[\left(u_j - \frac{\partial \tilde{x}_j}{\partial t}\right)T\right] = k_g \frac{\partial^2 T}{\partial x_j^2} \tag{8c}$$

Conservation of dilute chemical species

$$\frac{\rho_g}{\sqrt{g}}\frac{\partial}{\partial t}(\sqrt{g}\omega_s) + \rho_g \frac{\partial}{\partial x_j}\left[\left(u_j - \frac{\partial \tilde{x}_j}{\partial t}\right)\omega_s\right] = \rho_g D_s \frac{\partial^2 \omega_s}{\partial x_j^2} \tag{8d}$$

In these equations, $\tilde{x}_i$ represents the moving mesh location and $\sqrt{g}$ is the metric tensor determinate of the transformation, i.e., the local computational control-volume size. As such, terms of the form $\frac{\rho_g}{\sqrt{g}}\frac{\partial}{\partial t}(\phi\sqrt{g})$ account for the gain or loss of the variable $\rho_g\phi$ due to control-volume motion. For a stationary mesh, $\sqrt{g} = 1$ and $\partial\tilde{x}_j/\partial t = 0$.

Once the flow field is determined, heat and mass fluxes are computed at the gas–liquid interface using the gas-phase surface gradients, i.e.,

$$q_{conv} = -k_g \left.\frac{\partial T}{\partial n}\right|_{surf} \quad \text{and} \quad n_s = \frac{-\rho_g D_s \frac{\partial \omega_{s,surf}}{\partial n}}{(1-\omega_{s,surf})} \tag{9a,b}$$

These flux values are then applied to determine the area-averaged transient heat and mass transfer parameters,

$$h = \frac{\int_{surf} q_{conv}\,dA}{A(T - T_\infty)} \quad \text{and}$$

$$h_m = \frac{\int_{surf} n_s\,dA}{A\rho_g(\omega_{s,surf} - \omega_{s,\infty})/(1-\omega_{s,surf})} \tag{10a,b}$$

which are written in non-dimensional form as the Nusselt ($Nu \equiv hd/k_g$) and Sherwood ($Sh \equiv h_m d/D_s$) numbers.

Assumptions of thermodynamic equilibrium at the droplet surface, ideal gas conditions, and Raoult's law have been made such that the gas-phase surface concentrations can be expressed as

$$\omega_{s,surf} = \frac{x_s P_{sat,s}(T_d)}{\rho_g R_s T_d} \tag{11}$$

In the above expression, x_s is the liquid-phase mole fraction of component s, taken to be unity for a single component droplet, R_s is the gas constant, and $P_{sat,s}(T_d)$ is the temperature dependent saturation pressure. To estimate the saturation pressure on the surface, the Clausius–Clapeyron equation has been employed, i.e.,

$$P_{sat,s}(T_d) = P_{0,s}\exp\left[\frac{L_s}{R_s}\left(\frac{1}{T_{0,s}} - \frac{1}{T_d}\right)\right] \tag{12}$$

where $P_{0,s}$ and $T_{0,s}$ represent saturation conditions at a reference state.

Statements for the conservation of energy and mass, Eqs. (1) and (2), represent a coupled set of ordinary differential equations that can be solved for droplet temperature and radius over time. With the semi-empirical approach, heat and mass transfer parameters are readily available for a specified uniform flow particle Reynolds number such that multiple-point predictor–corrector algorithms can easily be used to solve the coupled ODE set. As such, a fourth-order Runge Kutta algorithm [35] has been implemented for ODE-based semi-empirical solutions to compute droplet flux values, temperature, radius, and mass over time for single component droplets. Variable time-step and error control routines have been included to ensure efficient and accurate solutions. The error control algorithm ensures that differences among solutions calculated using variable time increments Δt and $2\times\Delta t/2$ are negligible at each step [35,36].

For evaluation of Nusselt and Sherwood number conditions, the computational fluid dynamics program CFX 4.4 (ANSYS, Inc.), which is a finite-volume code that allows for multiblock structured meshes, has been implemented to solve the flow field conservation equations. Mesh deformation has been included to account for the effects of droplet evaporation. To improve computational accuracy on the scales of interest, a cgs (centimeters, grams, and seconds) system of units and double precision calculations have been employed. All flow field equations have been discretized to be at least second-order accurate in space. The third-order QUICK scheme has been employed for the advection terms in order to better resolve the upstream diffusional effects that arise for the lower Reynolds number flows of interest. The use of moving grids to resolve droplet evaporation limits temporal discretization to first-order accuracy, i.e., a fully implicit backward Euler scheme. However, time-step size and not method order determine *solution* accuracy, such that an acceptable solution can be achieved for a sufficiently small time-step.

Once the gas-phase heat, mass, and flow fields have been determined for a time-step, the effects on the particle are evaluated. Convective and mass fluxes are computed at the droplet surface using Eqs. (9a and b). Surface gradients of temperature and mass fraction have been computed to be second-order accurate on the deformable non-uniform grid surrounding the droplet [37]. Given the use of a first-order method in time for the flow field equations, a first-order Euler approximation has also been used to determine the droplet temperature and remaining mass at each solution step. Due to numerical accuracy, it is most effective to next determine

the new droplet volume, composite density, and finally the diameter and mixture specific heat. Equations (10a and b) are then used to calculate the area-averaged heat and mass transfer parameters at the current time-step. Based on the new spherical diameter, the mesh resolving the flow field around the droplet is adjusted. The procedure is then advanced by setting the new droplet temperature and mass fraction at the spherical surface and repeating the flow field solution.

To resolve diffusion on the micron-size spatial scales of the droplets, a very small time-step is needed. Furthermore, the use of moving grids and the fully implicit backward Euler scheme severely limit the allowable time-step size. Using numerical experimentation, it was found that initial resolution of the developing gas-phase temperature and mass concentration profiles, along with accurate prediction of droplet temperature changes, required a time-step on the order of $\Delta t = 2\times10^{-4}$ s for the resolved volume approach. Considering that droplet evaporation often requires minutes to several hours, the associated number of time-steps is prohibitively large. However, it was found that once pseudo-steady temperature and concentration fields developed, time-steps could be increased significantly as further evaporation occurs. The upper limit for time-step size after pseudo-steady concentration fields have developed was found to be on the order of $\Delta t \approx 0.1$ s.

The external flow system of an isolated droplet represents a large flow environment with a relatively small disturbance field, especially for the higher Reynolds number flows considered. As such, significant residual reductions of all equations are required to ensure convergence. Numerical experimentation indicated that convergence could be assumed, based on a 1% relative local error criterion on all variables, once initial global residual values had been reduced by five to six orders of magnitude. In addition, the rate of residual reduction was also observed and used to establish convergence for all equations. While strict residual criteria had to be enforced for the external flow field compared to typical internal conditions, increased under-relaxation factors were allowable for the low Reynolds number solutions and reduced the number of iterations required to reach convergence, thereby decreasing solution time.

2.3. Geometry and boundary conditions

Two droplet evaporation systems have been investigated for the respiratory aerosol conditions of interest. To assess uniform flow effects only, a system consisting of a 2-D axisymmetric droplet in an infinite medium has been employed (Fig. 1a). A closed system was formulated by specifying walls far from the droplet in a manner that does not interfere with heat and mass transfer characteristics. Uniform flow was specified

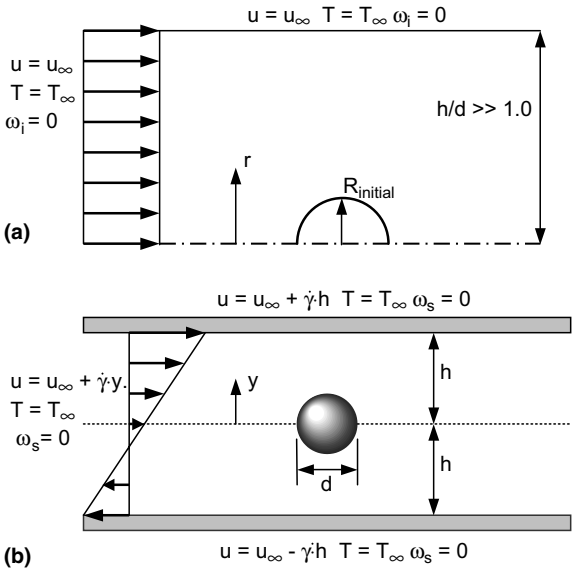

Fig. 1. Droplet evaporation systems: (a) axisymmetric two-dimensional geometry of a spherical droplet in a nearly infinite media subjected to uniform flow u_∞; and (b) three-dimensional geometry of a spherical droplet in the presence of centerline flow (u_∞), linear shear ($\dot{\gamma}$), and perfectly absorbing boundaries.

sufficiently far upstream from the droplet to represent motion relative to the surrounding air, i.e., particle slip.

To evaluate the effects of linear shear stress and wall proximity on droplet evaporation, a 3-D spherical droplet has been considered near planar wall boundaries (Fig. 1b). This system is characterized by a droplet of diameter d located equal distance h from two infinite flat walls. The flow field upstream of the droplet is composed of both uniform velocity (u_∞) and planar shear ($\dot{\gamma}y$) components. The imposed uniform velocity accounts for the relative motion of the particle in the flow field. The planar shear flow is consistent with local flow field conditions and is not a relative term. To avoid disturbances in the linear shear field, slip has been allowed on the walls. Stated another way, the walls have been assigned a velocity consistent with the local fluid velocity.

For both systems considered, zero mass concentration, or perfect absorption, and ambient temperature conditions have been specified on the lateral boundaries and upstream of the droplet. While slip is allowed on the walls, the droplet surface is considered rigid due to high relative surface tension forces resulting in a no-slip boundary condition. Droplet surface temperature is assumed spatially constant and is specified according to initial and previous time-step conditions. Based on droplet temperature, saturation pressure is determined for each species from the Clausius–Clapeyron equation and is used to calculate the constant gas-phase surface

concentration (Eqs. (11) and (12)). For the 3-D planar shear case, the assumption of a perfectly absorbing wall allows for the true relative velocity between the particle and wall to be ignored. That is, the wall as viewed by the particle is constant and unchanging with time.

For respiratory aerosols, conditions of interest include particle diameters $5 \leqslant d \leqslant 300$ μm, uniform flow Reynolds numbers $0 \leqslant Re_p \equiv \rho u_\infty d/\mu \leqslant 8$ and shear-based Reynolds numbers $0 \leqslant Re_g \equiv \rho \dot{\gamma} d^2/\mu \leqslant 32$. Flow field similarity is expected across the diameter range considered for comparable Reynolds number conditions and h/d values provided non-continuum effects and particle deformation are avoided. Non-continuum flow effects on heat and mass transfer are expected to be minimal for diameters greater than 5 μm [8]. For the maximum particle Reynolds numbers and diameters considered, the droplet Weber and Capillary numbers are less than 10^{-4}, which indicates dominance of the surface tension forces, such that spherical droplets may be assumed. Hence, a constant initial droplet diameter was selected and evaluated for wall distances of $h/d = 1$, 2, 5, and 10. Particle–wall separations smaller than one diameter have not been evaluated due to flow instabilities arising at the higher Reynolds numbers considered and potential non-continuum effects for particle–wall separation distances less than approximately 5 μm [38].

The non-linear multivariable regression analysis required to generate Sherwood number correlations for the conditions of interest has been conducted using Datafit (Oakdale Engineering, Oakdale, PA) and JMP 4 (SAS Institute, Cary, NC) statistical software.

3. Results

3.1. Velocity fields and scalar transport

For the 2-D axisymmetric geometry (Fig. 1a), representative velocity vectors, contours of velocity magnitude and mass fractions for an *n*-heptane droplet in air ($T_\infty = 298$ K and $Re_p = 30.2$) far from a boundary are shown in Fig. 2a and b. Moderate momentum diffusion due to viscous forces results in noticeable flow field influences upstream of the droplet and rapid downstream recovery of a uniform velocity profile. Upstream mass diffusion is much less pronounced due to the relatively high Schmidt number of *n*-heptane in air ($Sc = 2.4$) and the contour levels selected. For the 3-D wall-bounded geometry (Fig. 1b), representative velocity vectors, contours of velocity magnitude and mass fractions are shown in Fig. 2c and d under concurrent centerline flow and shear conditions ($Re_p = 1.0$ and $Re_g = 4.0$).

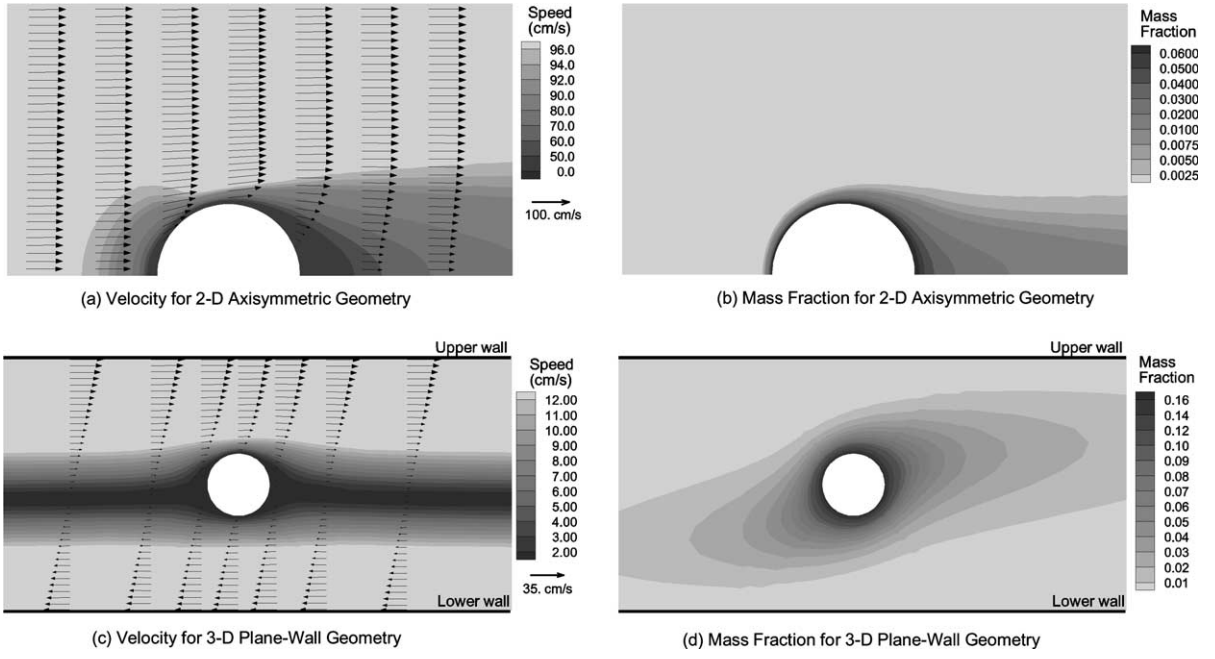

Fig. 2. Representative flow field results: (a) velocity vectors, contours of velocity magnitude, and (b) mass fraction for an axisymmetric *n*-heptane droplet far from the wall with $T_\infty = 298$ K and $Re_p = 30.2$. (c) Velocity vectors, contours of velocity magnitude, and (d) mass fraction for a three-dimensional *n*-heptane droplet subjected to non-uniform plane shear flow ($Re_p = 1.0$, $Re_g = 4.0$) and wall effects ($h/d = 2.0$) with $T_\infty = 298$ K. Asymmetry of the mass contours arises from the non-zero centerline velocity, and increases with Re_p for non-zero Re_g.

Asymmetry of the mass contours arises from the non-zero centerline velocity, and increases with Re_p for non-zero Re_g. In addition, the mass contours indicate that wall proximity likely has little effect on droplet evaporation for this case.

3.2. Model validation

To validate the semi-empirical and resolved volume approaches for uniform flow, evaporation results have been compared to the experimental measurements of Runge et al. [39] for conditions similar to respiratory aerosols. Runge et al. [39] considered the evaporation of hydrocarbon droplets under uniform flow conditions characterized by $30 \leqslant Re_p \leqslant 127$, $d = 600$ μm and $T \leqslant 300$ K. While these conditions do not match the exact diameters and Reynolds numbers expected for respiratory aerosols, similarity can be assumed based on particle Reynolds numbers below the onset of vortex shedding ($Re_p \leqslant 130$) and droplet deformation [8]. Furthermore, significant internal temperature and concentration gradients are more likely to arise for the higher particle Reynolds number conditions of the Runge et al. [39] data. Therefore, matching comparisons between these empirical results and evaporation models should instill confidence that the rapid mixing model assumptions are valid for respiratory aerosol conditions, as verified by Longest and Kleinstreuer [28]. Consistent with the uniform flow experiments of Runge et al. [39], *n*-heptane droplets have been considered in this study, which are similar in volatility to common toxic (benzene) and therapeutic (HFA 134a) respiratory aerosols.

Semi-empirical and resolved volume simulations of an *n*-heptane droplet evaporating at $T_\infty = 272$ K and $Re_p = 107.3$ are shown to closely match the empirical results of Runge et al. [39] in Fig. 3a. The mild over-prediction of the models may be due to a violation of the rapid mixing model or constant property assumptions for the elevated mass flux conditions. However, this discrepancy is negligible and not expected for the lower Reynolds numbers and diameters of respiratory aerosols. In comparison to the resolved volume simulation, the mild decrease in evaporation rate predicted by the semi-empirical model is likely due to differences in the empirical Sherwood and Nusselt number correlations and full resolution of the surface gradients.

Considering droplet temperature, rapid cooling occurs until the droplet wet-bulb condition is reached and then remains relatively constant at a pseudo-steady-state, due to the balance between evaporative heat loss and convective effects under constant external flow conditions. In comparison to the experimental results of Runge et al. [39] for the *n*-heptane droplet considered in Fig. 3a, the resolved volume solution matches the observed droplet temperatures very well (Fig. 3b).

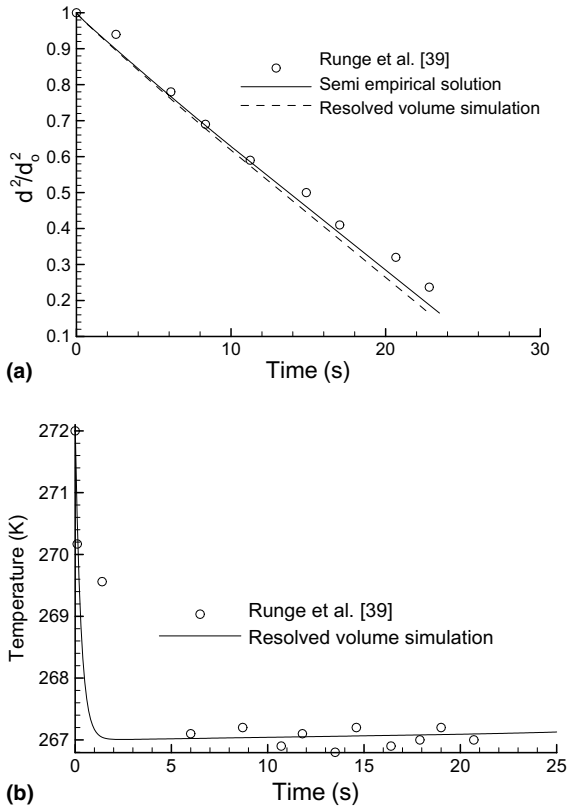

Fig. 3. Comparisons of computational estimates with experimental results of Runge et al. [39] including (a) normalized droplet surface area (d^2/d_0^2) through time for *n*-heptane with $T_\infty = 272$ K and $Re_p = 107.3$; and (b) spatially constant droplet temperature over time for *n*-heptane with $T_\infty = 272$ K and $Re_p = 107.3$.

Similar performance is also observed for the semi-empirical-based approach.

The empirical Sherwood and Nusselt number correlations provided by Ranz and Marshall [32] and Clift et al. [8] were formulated for wide ranges of particle Reynolds numbers and may not be highly accurate for the uniform flow conditions of respiratory aerosols. To evaluate the applicability of these empirical correlations, resolved volume simulations of uniform flow in the 2-D and 3-D systems have been used to compute Sherwood and Nusselt numbers in the range of $0 \leqslant Re_p \leqslant 30$. Considering Sherwood number values, the correlation of Clift et al. [8] provides the best fit to the numerical data (Fig. 4a). The Ranz and Marshall [32] correlation marginally over predicts the Sherwood values for particle Reynolds numbers less than approximately 2, which is consistent with the originally specified range of $2 \leqslant Re_p \leqslant 200$. Retaining the widely used form of the Ranz and Marshall [32] correlation, a best fit to the numeric Sherwood data in the range of $0 \leqslant Re_p \leqslant 30$ results in

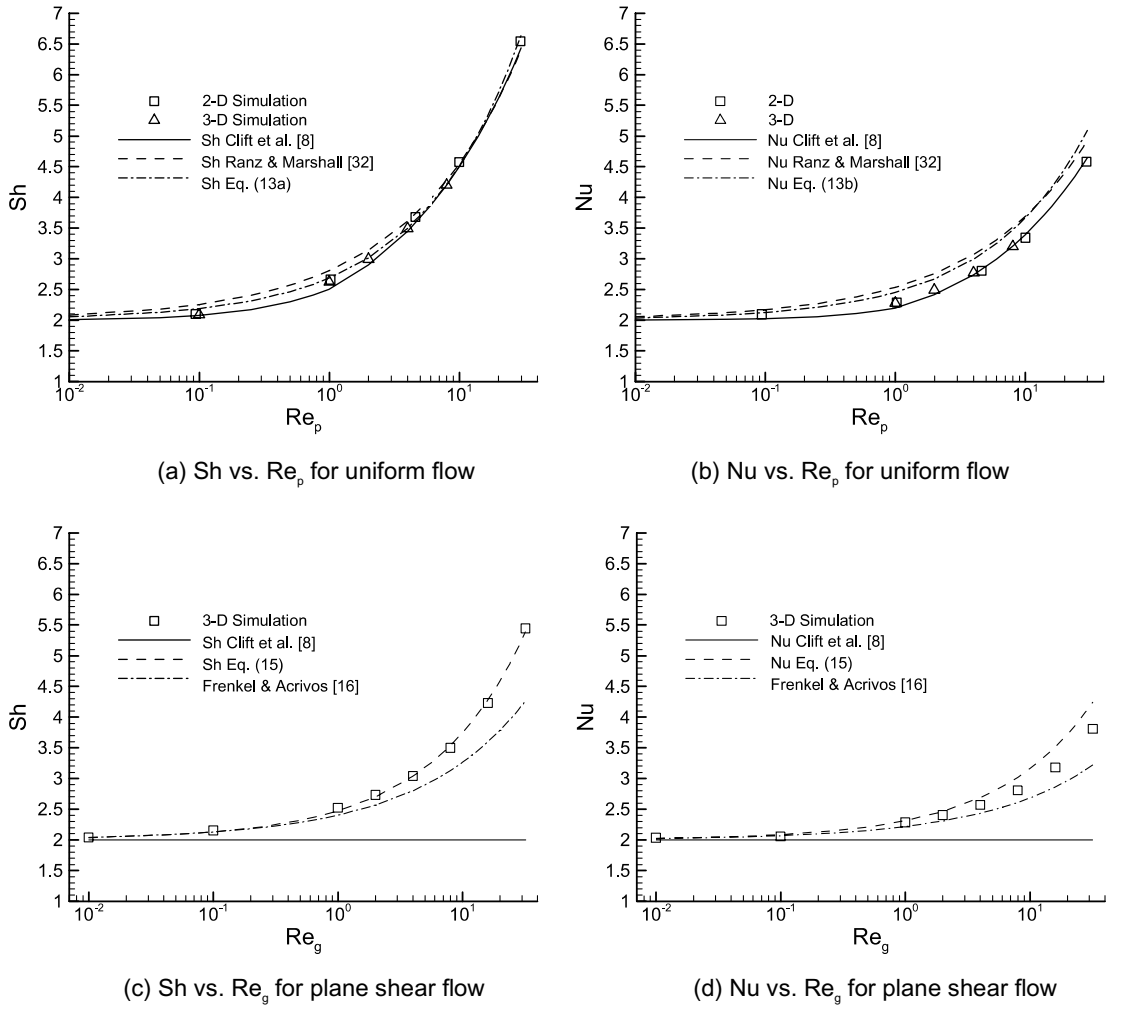

Fig. 4. Comparisons of simulated and empirical results: (a) Sherwood and (b) Nusselt numbers for uniform flow ($Re_p \geqslant 0$ and $Re_g = 0$); and (c) Sherwood and (d) Nusselt numbers under plane shear conditions ($Re_p = 0$ and $Re_g \geqslant 0$).

$$Sh = 2.0 + 0.474 Re_p^{0.6} Sc^{0.333} \tag{13a}$$

This relation provides an improved representation of the data ($R^2 = 0.99$ and p-value $\leqslant 0.01$), especially in the critical range of $Re_p \approx 1$. Considering Nusselt number values, the more complex expression of Clift et al. [8] again provides the best fit to the numerical results (Fig. 4b). Applying the heat and mass transfer analogy, a Nusselt number relation comparable to Eq. (13a), can be written

$$Nu = 2.0 + 0.474 Re_p^{0.6} Pr^{0.333} \tag{13b}$$

This expression results in improved Nusselt number predictions in the range of $Re_p \approx 1$ compared to the Ranz and Marshall [32] correlation. While Nusselt number estimates calculated using Eq. (13b) are marginally higher than the simulated values, the effect on the evaporation rate is not expected to be large considering the relatively mild temperature variations of interest. Furthermore, Eqs. (13a and b) are simpler than the expressions of Clift et al. [8] and represent a more familiar form. As such, Eqs. (13a and b) will be used to describe the uniform flow contribution to heat and mass transfer for respiratory aerosol conditions.

3.3. Effect of shear flow (Re_g)

In the absence of uniform flow and wall interactions, the effects of shear rate on droplet Sherwood and Nusselt number values as computed from the 3-D model are shown in Fig. 4c and d. As indicated in these figures, the uniform flow expression of Clift et al. [8] does not account for the potentially significant effect of shear rate on the Sherwood and Nusselt number correlations.

Frenkel and Acrivos [16] used perturbation theory to derive a low Re_g approximation for variations in the Sherwood number, i.e.,

$$Sh = 2.0 + 0.4552\left(\frac{Re_g Pr}{\pi}\right)^{0.5} + O(Re_g \cdot Pr) \tag{14}$$

which appears accurate for $Re_g \leqslant 1$ (Fig. 4c). For the range of shear values considered, curve fitting the numerical results through $Re_g = 32$ in a form consistent with the uniform flow correlation of Ranz and Marshall [32] results in

$$Sh = C_1 + C_2 Re_g^{C_3} Sc^{0.333} \tag{15a}$$

where

$$C_1 = 2.0; \quad C_2 = 0.35; \quad C_3 = 0.57 \tag{15b–d}$$

The associated Nusselt number correlation formed by interchanging the Prandtl and Schmidt numbers provides a reasonably accurate result in comparison to numerical estimates (Fig. 4d).

Based on the numerical data, it appears that planar wall shear begins to affect Sherwood number values for $Re_g \geqslant 0.05$. For a near-wall shear rate of $\dot{\gamma} = 6000$ s^{-1}, shear-based Reynolds numbers for 10 and 100 μm respiratory aerosols are approximately 0.05 and 4, respectively. Therefore, planar shear is expected to have a negligible effect on respiratory aerosols less than 10 μm. In contrast, planar shear may increase the Sherwood number of inhaled 100 μm aerosols by 50% and 300 μm aerosols by 175% in the upper respiratory tract.

3.4. Effects of shear flow (Re_g) and wall proximity (h/d)

In the absence of uniform flow, the combined effects of planar shear stress and near-wall proximity are illustrated in Fig. 5. For zero flow conditions, the wall has a discernable effect on the Sherwood number for $h/d = 5$ and practically no effect for $h/d = 10$. At low shear Reynolds numbers, diffusion from the droplet into the wall significantly enhances mass transport resulting in elevated Sherwood values for near-wall spacings. As the shear Reynolds number is increased, convective transport sweeps concentration profiles downstream such that the effect of near-wall diffusion is reduced. Around $Re_g = 8$, the wall has little effect on heat transfer for all particle–wall separations considered. Beyond a Re_g value of 8, near-wall proximity effectively reduces the Sherwood values due to compression of streamlines above and below the particle. The combined effects of planar shear and wall proximity can be represented in

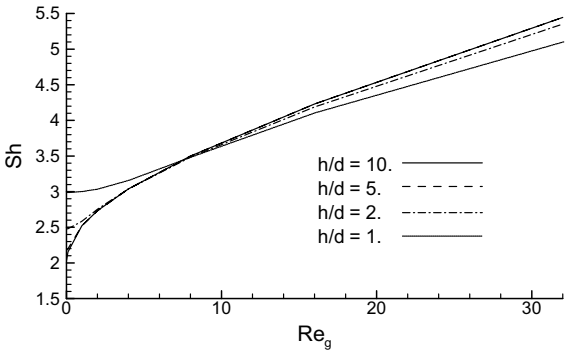

Fig. 5. Effects of wall proximity (h/d) on the Sherwood number for plane shear flow conditions ($Re_p = 0$ and $Re_g \geqslant 0$).

the form of a correlation consistent with Eq. (15a) as follows

$$Sh = C_1 + C_2 Re_g^{C_3} Sc^{0.333} \tag{16a}$$

where for $1 \leqslant h/d < 10$

$$C_1 = 1.92 + \frac{1.03}{h/d} \tag{16b}$$

$$C_2 = 0.42 \exp\left(\frac{-2.08}{h/d}\right) \tag{16c}$$

$$C_3 = 0.53 + \frac{0.47}{h/d} \tag{16d}$$

The correlation coefficient and p-value for the above relation are $R^2 = 0.99$ and $p < 0.001$. These shear flow correlations are summarized in Table 1 for both $h/d \geqslant 10$ and $1 \leqslant h/d < 10$.

3.5. Effects of uniform flow (Re_p) and shear (Re_g)

Results of the combined effects of uniform and plane shear flows on a particle far from a boundary ($h/d \geqslant 10$) are shown in Fig. 6 for the conditions of interest. Clearly, the familiar curve for the Sherwood number as a function of Re_p is altered in a non-linear manner for increasing values of Re_g. Nusselt number values follow a similar but more compressed pattern, due to a non-zero Lewis number. The following correlation has been fit to the numerically generated data and accounts for non-linear variations in the Sherwood number associated with combined uniform and plane shear flows for $h/d \geqslant 10$

$$Sh = \underbrace{C_1 + C_2 Re_g^{C_3} Sc^{0.333}}_{\text{Shear flow term}} \underbrace{+0.474 Re_p^{0.6} Sc^{0.333}}_{\text{Uniform flow term}} \underbrace{\exp(-C_4 \cdot Re_g) + \left(\frac{Re_p}{C_5}\right)^2 (1 - \exp(-C_4 \cdot Re_g))}_{\text{Exponential interaction terms}} \tag{17a}$$

Table 1
Effects of uniform flow, shear, and near-wall proximity on the evaporation of respiratory aerosols

	Sherwood number correlation	Coefficients for $h/d \geqslant 10$	Coefficient for $1 \leqslant h/d < 10$	Single wall correction
Uniform flow	$Sh = C_1 + C_2 Re_p^{C_3} Sc^{0.333}$	$C_1 = 2.0$ $C_2 = 0.474$ $C_3 = 0.6$	[a]	[a]
Shear flow	$Sh = C_1 + C_2 Re_g^{C_3} Sc^{0.333}$	$C_1 = 2.0$	$C_1 = 1.92 + \frac{1.03}{h/d}$	Replace h with $2h_1$
		$C_2 = 0.35$	$C_2 = 0.42 \exp\left(\frac{-2.08}{h/d}\right)$	
		$C_3 = 0.57$	$C_3 = 0.53 + \frac{0.47}{h/d}$	
Interacting uniform and shear flow	$Sh = C_1 + C_2 Re_g^{C_3} Sc^{0.333} + 0.474 Re_p^{0.6} Sc^{0.333} \exp(-C_4 \cdot Re_g) + \left(\frac{Re_p}{C_5}\right)^2 (1 - \exp(-C_4 \cdot Re_g))$	$C_1 = 2.0$	$C_1 - C_3$ from shear flow correlation	Replace h with $2h_1$
		$C_2 = 0.35$ $C_3 = 0.57$		
		$C_4 = 0.37$	$C_4 = \frac{h/d}{-9.35 + 0.82 h/d + 8.55\sqrt{h/d}}$	
		$C_5 = 11.14$	$C_5 = 11.21 - \frac{2.89}{(h/d)^2}$	

[a] Can be approximated from interacting flow relation with $Re_g = 0$.

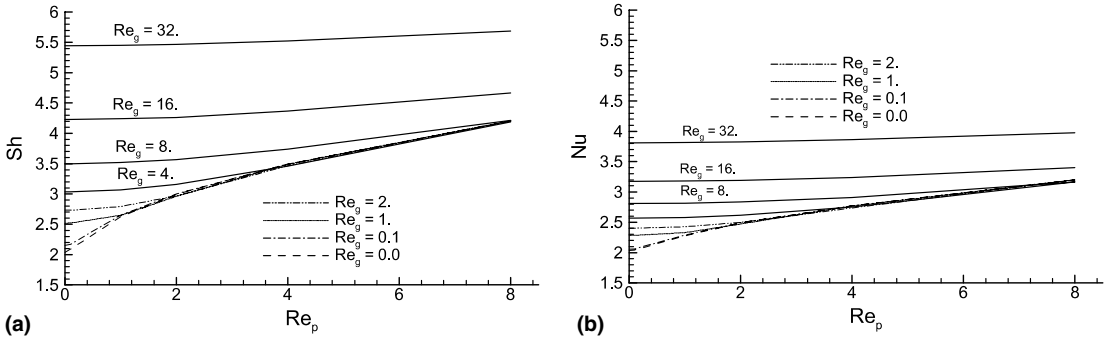

Fig. 6. (a) Sherwood number and (b) Nusselt number versus Re_p for variable shear rates ($Re_g \geqslant 0$) with $h/d \geqslant 10$.

Constants C_1, C_2 and C_3 are given as Eqs. (15b–d). The remaining coefficients are

$$C = 0.37; \qquad C_5 = 11.14 \tag{17b,c}$$

The above correlation is an appropriate fit to the numeric data, as represented by $R^2 = 0.97$ and $p < 0.001$. This relation reduces to Eq. (13a) for uniform flow ($Re_g = 0$) and Eq. (15a) for pure shear flow ($Re_p = 0$) (cf. Table 1). The exponential interaction terms account for the non-linear flow effects that arise for the particle and shear Reynolds numbers of interest.

3.6. Effects of uniform flow (Re_p), shear (Re_g), and wall proximity (h/d)

Respiratory aerosols are often exposed to high shear near-wall conditions in which particle slip is enhanced. Joint effects of these three mechanisms on particle mass transfer are illustrated in Fig. 7. For particles five diameters from the surface, a small wall effect is perceivable at low Re_g and Re_p values (Fig. 7a versus Fig. 7b). For $h/d = 2$, the presence of the wall results in an increase in Sherwood number values for $Re_p \leqslant 2$ and $Re_g \leqslant 4$ (Fig. 7c). Finally, for particles one diameter from the wall, a significant increase in Sherwood values is observed for most Re_p values and $Re_g < 8$ (Fig. 7d). For Re_g values greater than 8 and $h/d = 1$, Sherwood values are reduced significantly for small values of Re_p. To fit a correlation to the numeric data for concurrent uniform flow, shear, and near-wall effects, the form of Eq. (17a) has been implemented. Coefficients $C_1 - C_5$ have been used to account for near-wall proximity. To remain consistent with Eq. (16a), coefficients $C_1 - C_3$ are given by

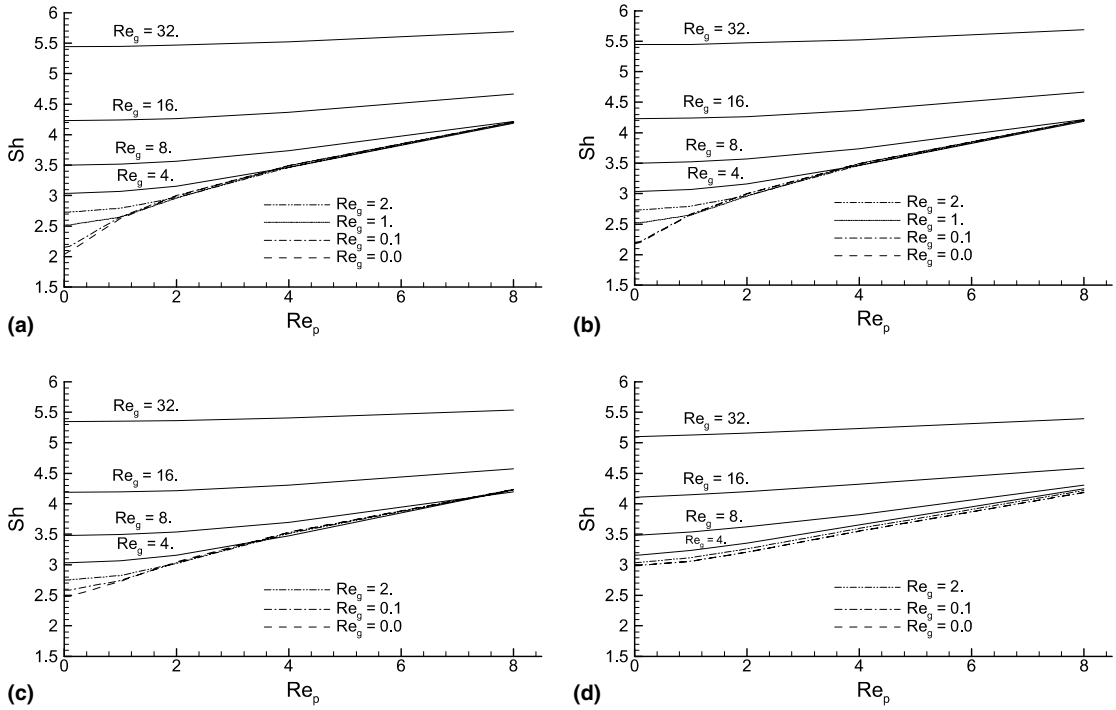

Fig. 7. Sherwood number versus Re_p with variable shear rates ($Re_g \geqslant 0$) for (a) $h/d = 10$, (b) $h/d = 5$, (c) $h/d = 2$, (d) $h/d = 1$.

Eqs. (16b–d). The remaining coefficients are represented as

$$C_4 = \frac{h/d}{-9.35 + 0.82h/d + 8.55\sqrt{h/d}} \quad \text{and}$$

$$C_5 = 11.21 - \frac{2.89}{(h/d)^2} \tag{18a,b}$$

The overall fit of this model to the data is described by $R^2 = 0.92$ and $p < 0.001$, and the coefficients are summarized in Table 1. Comparison of predicted and numeric values of the Sherwood number indicates a reasonably good fit with the most significant error occurring for the maximum considered values of both Re_p and Re_g.

For comparable Nusselt number estimates, the above equations may be modified by replacing the Schmidt number with the Prandtl number. Implementing the heat and mass transfer analogy, Nusselt number estimates were found to be within 10% of numerical values except for the single data point of $Re_p = 8$ and $Re_g = 32$.

Specifying a system consisting of two equally spaced boundaries simplifies the numerical analysis of planar effects by avoiding excessively high velocities at positions far removed from the droplet for the larger Re_g values of interest. However, a near-wall aerosol in the upper respiratory tract is characterized by the presence of a single absorbing boundary. To address this issue, the Sherwood number correlations developed can be applied to a single boundary scenario by replacing the value of h with $2 \cdot h_1$, where h_1 is the separation distance between the particle and the single wall boundary (Table 1). This substitution effectively reduces the influence of the wall by a factor of 2. Representative simulations of single wall conditions at high and low values of Re_p and Re_g indicate that this approximation is reasonably accurate with deviations approaching only 5% for high Re_p and Re_g values.

4. Discussion

In this study, the interacting effects of uniform flow, plane shear, and near-wall proximity on spherical droplet heat and mass transfer have been assessed. Validated resolved volume simulations were performed to determine Sherwood and Nusselt number values for non-uniform and near-wall flow conditions consistent with inhalable aerosols in the upper respiratory tract. Multivariable non-linear regression was employed to develop Sherwood and Nusselt number correlations for use in efficient semi-empirical droplet evaporation models. For the respiratory aerosol conditions of interest, assumptions implemented include rigid spherical non-rotating droplets, constant gas-phase properties, and rapid mixing within the liquid resulting in no internal gradients. While not directly assessed in this study, other factors that may influence the evaporation of respiratory

aerosols include non-continuum flow effects and multicomponent liquids.

Other studies have considered the influence of plane shear on particle heat and mass transfer for creeping flow conditions [16], as well as the interacting effects of plane shear and near-wall proximity [22]. However, this study is the first to quantify the interacting effects of uniform flow, plane shear and near-wall proximity for low Reynolds number conditions extending beyond the creeping flow regime, which are typical of respiratory aerosols. Findings include a significant influence from planar shear that should be included beyond a shear-based Reynolds number of approximately 1. Due to the d^2 term in the numerator of the shear Reynolds number, values above unity will typically only occur for inhaled aerosols greater than 50 μm under non-uniform flow and near-wall conditions. Wall proximity significantly enhanced heat and mass transfer due to conduction and diffusion at small separation distances ($h/d < 5$) and for small particle Reynolds numbers, the latter being more common for small particle diameters. Wall proximity was found to increase heat and mass transfer for Re_g values less than approximately 8 and otherwise reduced convective effects. In addition, strong non-linear interactions were observed between uniform and shear flows at all particle–wall separation distances for the Reynolds number conditions of interest. These interactions were most significant for similar values of the uniform flow and shear Reynolds numbers, and diminished for conditions in which one Reynolds number became approximately three times larger than the other.

The Sherwood and Nusselt number correlations developed in this study can be applied to more accurately compute hygroscopic and evaporative effects of aerosols in the respiratory tract using efficient semi-empirical models [10,27,31]. While *mean* residence times in the upper respiratory airways are very brief (e.g., 30 ms), Zhang et al. [3] showed that droplet evaporation rate had a significant impact on the deposition of inhaled JP-8 fuel aerosols. This effect is largely due to the increased residence time of near-wall particles in comparison to mean flow. Considering the findings of Zhang et al. [3] in conjunction with the increase in Sherwood and Nusselt numbers observed in this study, it is expected that individual and non-linear interacting effects of uniform flow, plane shear and near-wall proximity will significantly impact the transport and deposition of respiratory aerosols as well as the formation of aerosol derived vapors. Furthermore, the presence of the wall creates an additional drag force on the particle [36,38,40], which effectively increases the particle Reynolds numbers and should be taken into account when computing droplet evaporation rates and deposition.

The effects of non-continuum flow and multicomponent droplets, which frequently arise with respiratory aerosols, can be partially taken into account with the correlations developed in this study. Considering a droplet in air, non-continuum effects begin to become significant for diameters less than 5 μm [8]. Similar to the Cunningham correction factor for drag in rarified flows, theoretical and empirical correction factors have also been developed for heat and mass transfer. Clift et al. [8] suggested an empirical non-continuum correction factor to Sherwood and Nusselt numbers for uniform flow conditions. For a 5 μm droplet in air, the expression of Clift et al. [8] reduces the uniform flow Sherwood number by approximately 5%. However, this correction factor may not appropriately account for non-continuum effects on heat and mass transfer that arise for shear flow or at wall boundaries. To assess these conditions, corrections for the heat and mass flux terms are proved by Qu et al. [41,42]. Provided the rapid mixing model assumptions can be applied to multicomponent respiratory aerosols, including hygroscopic droplets, the Sherwood number correlation can be used to evaluate the condensation or evaporation of each individual component. Individual surface concentrations can be approximated using Eq. (13), which implements Raoult's law where x_s is the liquid-phase mole fraction of each droplet component.

The Sherwood and Nusselt number correlations developed in this study are limited to the assumptions employed by the resolved volume simulations, including rapid mixing and a constant property gas-phase. While these assumptions are generally applicable to respiratory aerosol conditions, exceptions may arise. For instance, highly volatile aerosols may rapidly evaporate when exposed to body temperature and upper airway flow conditions. Rapid evaporation may induce blowing velocity effects as well as variable gas-phase properties, which both may reduce evaporation rates. While blowing velocity was considered in the resolved volume equations, the single component droplet considered may not have evaporated at a rate sufficient for effects to impact the correlations. Further resolved volume simulations are needed to assess the potential effects of rapid evaporation on Sherwood and Nusselt number values, especially for highly volatile species.

In conclusion, resolved volume simulations have been employed to investigate the interacting effects of uniform flow, plane shear, and wall proximity on the heat and mass transfer of idealized spherical non-rotating droplets. Results indicate significant non-linear interactions among the non-uniform flows and near-wall conditions of interest. The resulting multivariable Sherwood and Nusselt number correlations can be used to efficiently compute the evaporation of single and multicomponent aerosols in the upper respiratory tract. Further numeric and experimental studies are needed to investigate conditions that may violate the assumptions of rapid mixing for multicomponent droplets and constant gas-phase properties for highly volatile liquids.

Acknowledgments

This effort was sponsored by the Air Force Office of Scientific Research, Air Force Material Command, USAF, under grant number F49620-01-1-0492 (Dr. Walt Kozumbo, Program Manager). The US Government is authorized to reproduce and distribute reprints for governmental purposes notwithstanding any copyright notation thereon. Use of the software package CFX4 from ANSYS, Inc. (Canonsburg, PA) and access to the SGI Origin 2400 at the North Carolina Supercomputing Center (RTP, NC) are gratefully acknowledged.

References

[1] T.B. Martonen, K.A. Bell, R.F. Phalen, A.F. Wilson, A. Ho, Growth rate measurements and deposition modeling of hygroscopic aerosols in human tracheo-bronchial models, Ann. Occupational Hyg. 26 (1982) 93–108.

[2] W.H. Finlay, K.W. Stapleton, The effect on regional lung deposition of coupled heat and mass transfer between hygroscopic droplets and their surrounding phase, J. Aerosol Sci. 26 (4) (1995) 655–670.

[3] Z. Zhang, C. Kleinstreuer, C.S. Kim, Y.S. Cheng, Vaporizing micro-droplet inhalation, transport and deposition in a human upper airway model, Aerosol Sci. Technol. 38 (2004) 36–49.

[4] D.M. Broday, P.G. Georgopoulos, Growth and deposition of hygroscopic particulate matter in the human lungs, Aerosol Sci. Technol. 34 (2001) 144–159.

[5] T.B. Martonen, J.D. Schroeter, Risk assessment dosimetry model for inhaled particulate matter: II. Laboratory surrogates, Toxicol. Lett. 138 (2003) 133–142.

[6] W.H. Finlay, The Mechanics of Inhaled Pharmaceutical Aerosols, Academic Press, San Diego, 2001.

[7] D.A. Edwards, C. Dunbar, Bioengineering of therapeutic aerosols, Ann. Rev. Biomed. Eng. 4 (2002) 93–107.

[8] R. Clift, J.R. Grace, M.E. Weber, Bubbles, Drops, and Particles, Academic Press, New York, 1978.

[9] S.S. Sadhal, P.S. Ayyaswamy, J.N. Chung, Transport Phenomena with Drops and Bubbles, Springer, New York, 1997.

[10] W.A. Sirignano, Fluid Dynamics and Transport of Droplets and Sprays, Cambridge University Press, Cambridge, 1999.

[11] R.G. Cox, H. Brenner, The lateral migration of solid particles in Poiseuille flow: I. Theory, Chem. Eng. Sci. 23 (1968) 147–173.

[12] B.P. Ho, L.G. Leal, Inertial migration of rigid spheres in 2-D unidirectional flows, J. Fluid Mech. 65 (1974) 365–400.

[13] P. Cherukat, J.B. McLaughlin, The inertial lift on a rigid sphere in a linear shear flow field near a flat wall, J. Fluid Mech. 263 (1994) 1–18.

[14] D.C.T. Pei, Effect of tunnel blockage and support on the heat transfer form spheres, Int. J. Heat Mass Transfer 12 (1969) 1707–1709.

[15] V.T. Morgan, Wall bounded droplet heat transfer, Adv. Heat Transfer 11 (1975) 199–264.

[16] N.A. Frenkel, A. Acrivos, Heat and mass transfer from small spheres and cylinders freely suspended in shear flow, Phys. Fluids 11 (1968) 1913–1918.

[17] H. Chiang, C. Kleinstreuer, Computational analysis of interacting vaporizing fuel droplets on a one-dimensional trajectory, Combust. Sci. Technol. 86 (1992) 289–309.

[18] H. Chiang, C. Kleinstreuer, Transient heat and mass transfer of interacting vaporizing droplets in a linear array, Int. J. Heat Mass Transfer 35 (10) (1992) 2675–2682.

[19] H. Chiang, C. Kleinstreuer, Numerical analysis of variable-fluid-property effects on the convective heat and mass transfer of fuel droplets, Combust. Flame 92 (1993) 459–464.

[20] H.A. Dwyer, P. Stapf, R. Maly, Unsteady vaporization and ignition of a three-dimensional droplet array, Combust. Flame 121 (2000) 181–194.

[21] D.S. Dandy, H.A. Dwyer, A sphere in shear flow at finite Reynolds number: effect of shear on particle lift, drag, and heat transfer, J. Fluid Mech. 216 (1990) 381–410.

[22] H. Nirschl, H.A. Dwyer, V. Denk, Three-dimensional calculations of the simple shear flow around a single particle between two moving walls, J. Fluid Mech. 283 (1995) 273–285.

[23] W. Stahlhofen, G. Rudolf, A.C. James, Intercomparison of experimental regional aerosol deposition data, J. Aerosol Med. 2 (1989) 285–297.

[24] International Commission on Radiological Protection, ICRP, Human Respiratory Tract Model for Radiological Protection, ICRP Publication 66, Elsevier Science Ltd., New York, 1994.

[25] American Conference of Industrial Hygienists, ACGIH, Threshold Limit Values and Biological Exposure Indices, ACGIH, Cincinnati, 1997.

[26] W.C. Hinds, Aerosol Technology: Properties, Behavior, and Measurement of Airborne Particles, second ed., John Wiley & Sons, New York, 1999.

[27] G. Chen, S.K. Aggarwal, T.A. Jackson, G.L. Switzer, Experimental study of pure and multicomponent fuel droplet evaporation in a heated air flow, Atomization Sprays 7 (1997) 317–337.

[28] P.W. Longest, C. Kleinstreuer, Computational models for simulating multicomponent aerosol evaporation in the upper respiratory airways, Aerosol Sci. Technol. (submitted for publication).

[29] H. Niazmand, B.D. Shaw, H.A. Dwyer, I. Aharon, Effects of Marangoni convection on transient droplet evaporation, Combust. Sci. Technol. 103 (1994) 219–233.

[30] R.B. Bird, W.E. Stewart, E.N. Lightfoot, Transport Phenomena, John Wiley & Sons, New York, 1960.

[31] S.K. Aggarwal, A.Y. Tong, W.A. Sirignano, A comparison of vaporization models in spray calculations, AIAA J. 22 (10) (1984) 1448–1457.

[32] W.E. Ranz, W.R. Marshall, Evaporation from drops, Chem. Eng. Prog. 48 (1952) 141–146 and 173–180.

[33] M. Renksizbulut, R. Nafziger, X. Li, A mass transfer correlation for droplet evaporation in high-temperature flows, Chem. Eng. Sci. 46 (9) (1991) 2351–2358.

[34] I.R. Hawkins, N.S. Wilkes, Moving grids in Harwell-FLOW3D, AEA-InTec-0608, 1991.

[35] W.H. Press, B.P. Flannery, S.A. Teukolsky, W.T. Vetterling, Numerical Recipes, second ed., Cambridge University Press, Cambridge, 1992.
[36] P.W. Longest, C. Kleinstreuer, J.R. Buchanan, Efficient computation of micron-particle dynamics including wall effects, Comput. Fluids 33 (2004) 577–601.
[37] J.C. Tannehill, D.A. Anderson, R.H. Pletcher, Computational Fluid Mechanics and Heat Transfer, second ed., Taylor and Francis, Washington, 1997.
[38] B. Dahneke, Diffusional deposition of particles, J. Colloid Interface Sci. 48 (3) (1974) 520–522.
[39] T. Runge, M. Meske, C.E. Polymeropoulou, Low-temperature vaporization of JP-4 and JP-8 fuel droplets, Atomization Sprays 8 (1998) 25–44.
[40] E. Loth, Numerical approaches for motion of dispersed particles, droplets and bubbles, Prog. Energy Combust. Sci. 26 (2000) 161–223.
[41] X. Qu, E.J. Davis, B.D. Swanson, Non-isothermal droplet evaporation and condensation in the near-continuum regime, Aerosol Sci. 32 (2001) 1315–1339.
[42] X. Qu, E.J. Davis, Droplet evaporation and condensation in the near-continuum regime, Aerosol Sci. 32 (2001) 861–875.